Computational Condensed Matter 21 (2019) e00428

Contents lists available at ScienceDirect

Computational Condensed Matter

journal homepage: http://ees.elsevier.com/cocom/default.asp

Regular article

First Brillouin zone-centre phonon frequencies and elastic stiffness of the $Ln_2Hf_2O_7$ (Ln = La, Nd, Sm and Eu) pyrochlore

A.K. Kushwaha [a, *], A. Bouhemadou [b], R. Khenata [c], A. Candan [d], S. Akbudak [e], Ş. Uğur [f]

[a] Department of Physics, K.N. Govt. P.G. College, Gyanpur, Bhadohi, 221304, India
[b] Laboratory for Developing New Materials and Theirs Characterizations, University Ferhat Abbas Setif 1, 19000, Setif, Algeria
[c] Laboratoire de Physique Quantique de La Matière et de Modélisation Mathématique (LPQ3M), Université de Mascara, 29000, Algeria
[d] Department of Machinery and Metal Technology, Ahi Evran University, Kırşehir, 40100, Turkey
[e] Department of Physics, Faculty of Arts and Sciences, Adiyaman University, 02100, Adiyaman, Turkey
[f] Department of Physics, Faculty of Science, Gazi University, 06500, Ankara, Turkey

ARTICLE INFO

Article history:
Received 6 June 2019
Received in revised form
6 September 2019
Accepted 6 September 2019

Keywords:
Lanthanide hafnium oxide
Phonon frequency
Mechanical properties

ABSTRACT

First Brillouin zone-centre phonon frequencies, elastic stiffness and mechanical properties of the $Ln_2Hf_2O_7$ [Ln: La, Nd, Sm and Eu] pyrochlore structure were predicted by using an eight parameter bond-bending force constant model. One of the preliminary results of our study is that all the examined compounds are mechanically stable, and the elastic stiffness constants, and bulk and shear moduli decrease in the following sequence: $La_2Hf_2O_7 \rightarrow Nd_2Hf_2O_7 \rightarrow Sm_2Hf_2O_7 \rightarrow Eu_2Hf_2O_7$. The Poisson's ratio reveals that the interatomic bonding of the studied compounds has an ionic character and their ionicity decreases when one moves from La to Eu. The elastic properties are anisotropic and the anisotropy increases from La to Eu. The Raman and infrared active and inactive modes of the studied materials were calculated. Our findings are in good accordance with the related available data.

1. Introduction

Materials with frustrated magnetic properties have been subject of interest both theoretically and experimentally for many years [1–6]. In recent years, the lanthanide hafnium oxides with pyrochlore structure have drawn an increasing interest owing to their various technological applications, such as high-permittivity dielectrics [7], thermal barrier coatings (TBC) [8], high temperature solid electrolyte fuel cells [9], actinides host materials for nuclear waste [10], oxidation catalysts [11], superconductivity [12], gas sensing [13], luminescence [14,15] and chemical durability [16].

Gupta el al [17]. used the short-range force constant model with five stretching and two bending force constants to compute the zone-centre Raman and infrared phonon frequencies for the $A_2Hf_2O_7$ [A: La, Nd, Sm and Eu] pyrochlore. Recently, Qi et al. [18] measured the vibrational and dielectric properties of $LaHf_2O_7$ pyrochlore. Kumar and Gupta [19] studied the dielectric and vibrational properties of the hafnates $RE_2Hf_2O_7$ [RE: La, Nd, Sm, Eu, Gd and Tb] pyrochlore through ab initio calculations. They also computed the zone-centre Raman and infrared phonon frequencies as well as the static and effective dynamical charges. They found that the studied compounds have a mixed ionic-covalent bonding. Liu and co-workers [20] investigated the structural stability, elastic properties and thermal conductivity of the $La_2T_2O_7$ [T: Ge, Ti, Sn, Zr, Hf] pyrochlore using Vanderbilt-type ultra-soft pseudopotential plane wave within the local density approximation as incorporated in the CASTEP code. Feng et al. [21,22] studied the electronic and mechanical properties, and thermal conductivity of zirconium pyrochlore $Ln_2Zr_2O_7$ (Ln = La, Pr, Nd, Sm, Eu and Gd) using first principles density functional theory.

The main objective of the present work is the prediction of the vibrational and elastic properties of the $Ln_2Hf_2O_7$ (Ln = La, Nd, Sm and Eu) compounds by employing the eight parameter bond-bending force constants model. The paper is organized as follows: in the next section, we describe the crystal structure and method of calculations. Section 3 presents and discusses the obtained results. Finally, we end up with a conclusion.

2. Crystal structure and computational methodology

The $LnHf_2O_7$ compounds crystalize in a cubic system, space group $Fd3m$ (O_h^7), with eight unit formulas in the unit cell. The

* Corresponding author.
E-mail address: kushwaha.ar@gmail.com (A.K. Kushwaha).

https://doi.org/10.1016/j.cocom.2019.e00428
2352-2143/

constituent atoms occupy the following Wyckoff positions: Ln: 16*d* (1/2, 1/2, 1/2), Hf: 16*c* (0, 0, 0), O1: 48*f* (*x*, 1/8, 1/8) and O2: 8*b* (3/8, 3/8, 3/8). The Hf cation is surrounded by six O1 (Oxygen atom located at the 48*f* Wyckoff position) while the Ln cation is surrounded by eight O2 (Oxygen atom located at the 8*b* Wyckoff position). The crystal structure of $Ln_2Hf_2O_7$ can be viewed as interpenetrating networks of HfO_6 octahedra and Ln_2O chains [23]. The crystal structure of $Ln_2Hf_2O_7$ is shown in Fig. 1. Results deduced from theoretical analysis of each unit cell of sub-lattices can be given as;

$$\text{Hf } 16(c) = A_{2u} + E_u + 2F_{1u} + F_{2u}$$

$$\text{Ln } 16(d) = A_{2u} + E_u + 2F_{1u} + F_{2u}$$

$$\text{O1 } 48(f) = A_{1g} + E_g + 2F_{1g} + 3F_{2g} + A_{2u} + E_u + 3F_{1u} + 2F_{2u}$$

$$\text{O2 } 8(b) = F_{1u} + F_{2g.}$$

The First Brillouin zone-centre (Γ-point) optical phonon modes for the space group *Fd*3*m* (O_h^7) are given by the following representation:

$$\Gamma = A_{1g} + E_g + 2F_{1g} + 4F_{2g} + 3A_{2u} + 3E_u + 8F_{1u} + 4F_{2u} \quad (1)$$

Where A_{1g}, E_g, $4F_{2g}$ and $7F_{1u}$ symbolize the active Raman and infrared modes while $2F_{1g}$, $3A_{2u}$, $3E_u$ and $4F_{2u}$ denote the inactive ones.

Using Taylor's series expansion, the potential energy ϕ can be given by the following expression:

$$\phi = \sum_{lmn}\left[\frac{1}{r}\left(\frac{d\phi}{dr}\right)_{|r|=|r_k|}\left\{r^o_{lmn}(S_{lmn}-S_o)+\frac{1}{2}|S_{lmn}-S_o|^2\right\}+\frac{1}{2}\left\{\frac{1}{r}\frac{d}{dr}\left(\frac{1}{r}\frac{d\phi}{dr}\right)\right\}_{|r|=|r_k|}\{r^o_{lmn}(S_{lmn}-S_o)\}^2\right] \quad (2)$$

where *l*, *m* and *n* represent the direction cosines of the line joining the central ion and the nearest neighbor ion, S_0 and S_{lmn} are the displacements of the central ion and its first neighbor ions from their normal positions, respectively, and $|\mathbf{r_k}|$ denotes the nearest neighbor distance.

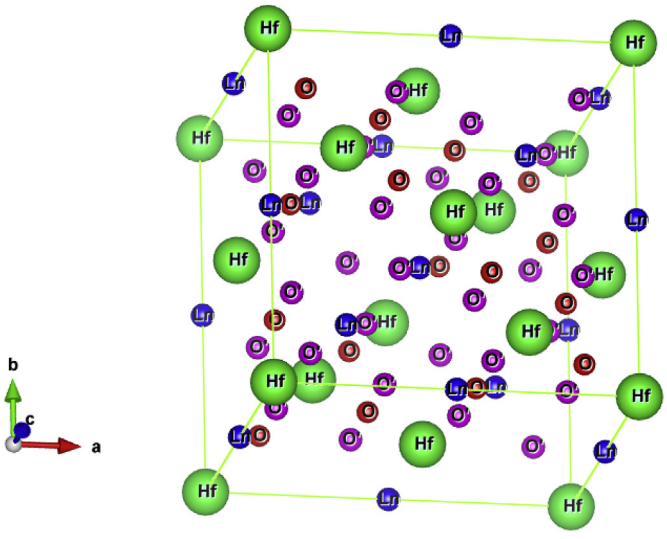

Fig. 1. Crystal structure of $Ln_2Hf_2O_7$ pyrochlore.

The A_k, which denotes the bond-stretching constant, can be derived from the potential energy φ as follows:

$$\frac{e^2}{V}A_k = \frac{d^2\phi}{dr^2}|_{|r|=|rk|} \quad (3)$$

The B_k, which denotes the bond-bending force constant, is expressed as the first derivative of the potential energy φ:

$$\frac{e^2}{V}B_k = \frac{1}{r}\frac{d\phi}{dr}|_{|r|=|r_k|} \quad (4)$$

Here, k = 1, 2, 3 and 4 for the first, second, third and fourth neighbors, respectively.

3. Results and discussion

3.1. Interatomic interactions and first Brillouin zone-centre phonons

In this study, we have considered that A_1 and B_1, A_2 and B_2, A_3 and B_3, and A_4 and B_4 are the bond-stretching and bond-bending interactions between the Hf and O1 atoms, Ln and O1 atoms, O1 and O1 atoms, and O1 and O2 atoms, respectively. The bond-stretching and bond-bending interactions have been calculated from the measured values of the zone-centre Raman mode A_{1g} [24] and the zone-centre infrared modes F_{1u} [25] for $La_2Hf_2O_7$, $Nd_2Hf_2O_7$ and $Sm_2Hf_2O_7$. For $Eu_2Hf_2O_7$, only the four experimental F_{1u} modes [25] are available in the literature, therefore, we have assumed that the four bond-bending force constants (B_1, B_2, B_3 and B_4) are equal to the average value of the corresponding force constants for the compounds $La_2Hf_2O_7$, $Nd_2Hf_2O_7$ and $Sm_2Hf_2O_7$. The calculated values are listed in Table 1. From Table 1, it is inferred that the first neighbor interactions between Hf and O1 atoms (Hf-O1) are stronger than those of the second and third neighbor ones. It is also noted that the interactions between the Hf and O1 atoms decreases in the sequence: $La_2Hf_2O_7 \rightarrow Nd_2Hf_2O_7 \rightarrow Sm_2Hf_2O_7 \rightarrow Eu_2Hf_2O_7$. The second neighbor interaction between the Ln and O1 atoms increases in the following order: $La_2Hf_2O_7 \rightarrow Nd_2Hf_2O_7 \rightarrow Sm_2Hf_2O_7 \rightarrow Eu_2Hf_2O_7$.

The zone-centre Raman and infrared active and inactive phonon modes for the studied compounds have been calculated from the calculated bond-stretching and bond-bending force parameters (given in Table 1), which were used as input data. The calculated zone-centre Raman and infrared active and inactive phonon modes are accommodated in Tables 2–4, respectively, along with available experimental [22,23] and theoretical [18,20,26,27] results. A

Table 1
Calculated force parameters (kdyn/cm) for $Ln_2Hf_2O_7$ (Ln = La, Nd, Sm and Eu).

Force constant	Internal coordinates	$LaHf_2O_7$	$Nd_2Hf_2O_7$	$Sm_2Hf_2O_7$	$Eu_2Hf_2O_7$
A_1	Hf–O	54.82	49.44	45.72	43.69
B_1	Hf–O	8.22	6.13	5.87	5.19
A_2	Ln-O	38.47	43.16	46.79	49.12
B_2	Ln-O	4.21	5.83	6.08	6.45
A_3	O–O	21.64	19.58	17.59	15.99
B_3	O–O	2.96	2.78	2.42	2.13
A_4	O–O′	18.76	16.79	15.23	13.88
B_4	O–O′	2.01	1.89	1.78	1.64

Table 2
Calculated Raman active modes for $Ln_2Hf_2O_7$ (Ln = La, Nd, Sm and Eu) along with available experimental and theoretical data.

System	A_{1g}	E_g	F_{2g} (1)	F_{2g} (2)	F_{2g} (3)	F_{2g} (4)
$La_2Hf_2O_7$						
This work	529	344	758	551	427	325
Exp. [22]	530	342	755	550	428	328
Exp. [23]	498		763	575	395	295
Cal. [19]	493	336	765	547	422	321
Cal. [17]	486	358	585	508	389	280
$Nd_2Hf_2O_7$						
This work	537	351	763	550	431	332
Exp. [22]	536	350		549	433	335
Exp. [23]	503		759	585	395	306
Cal. [19]	503	347	788	547	428	328
Cal. [17]	495	355	598	509	396	291
$Sm_2Hf_2O_7$						
This work	523	353	766	549	432	339
Exp. [22]	520			548	428	342
Exp. [23]			765	532	395	312
Cal. [19]	507	352	798	547	429	330
Cal. [17]	495	355	610	517	400	305
$Eu_2Hf_2O_7$						
This work	515	355	771	541	430	342
Exp. [22]				536	395	328
Cal. [19]	509	354	803	546	430	331
Cal. [17]	496	349	610	521	385	301

Table 3
Calculated infrared active phonon modes (cm^{-1}) for the $Ln_2Hf_2O_7$ (Ln = La, Nd, Sm and Eu) compound along with available experimental and theoretical data.

System	$F_{1u}(1)$	$F_{1u}(2)$	$F_{1u}(3)$	$F_{1u}(4)$	$F_{1u}(5)$	$F_{1u}(6)$	$F_{1u}(7)$
$La_2Hf_2O_7$							
This work	535	417	337	225	182	122	81
Exp. [22]	532	415	336	226	184	124	84
Exp. [18]	506	374	299	236	171	139	89
Cal. [18]	508	371	297	224	172	137	91
Cal. [19]	506	405	303	244	173	134	90
Cal. [17]	533	432	348	245	159	110	68
$Nd_2Hf_2O_7$							
This work	551	414	326	221	177	131	65
Exp. [22]	550	412	324	222	176	134	68
Cal. [19]	530	404	310	231	169	132	86
Cal. [17]	542	430	365	240	153	113	65
$Sm_2Hf_2O_7$							
This work	558	413	345	236	181	128	68
Exp. [2]	555	412	344	237	184	130	72
Cal. [19]	540	405	311	223	167	128	83
Cal. [17]	547	429	377	253	156	113	64
$Eu_2Hf_2O_7$							
This work	601	422	343	220	183	126	71
Exp. [22]	557	420	342	221			
Cal. [19]	545	406	311	219	166	125	81
Cal. [17]	551	441	362	244	153	113	66

comparison between theoretical and experimental Raman phonon modes for studied compounds is shown Fig. 2. The calculated values of the zone-centre phonon modes are in good agreement with available experimental results. From Table 1, one concludes that the interatomic interactions between the Hf and O1 atoms (first neighbor interactions) are much stronger than the interactions between the other constituent atoms, such as Ln−O1, O1−O1 and O1−O2 (second, third and fourth neighbor interactions) for $Ln_2Hf_2O_7$ [Ln = La, Nd, Sm and Eu]. Therefore, we can make an inference that the bonding between the Hf and O1 atoms is more ionic than that of the bonding between the other constituent atoms.

Fig. 3 represents the phonon dispersion spectra for the studied pyrochlore compounds $La_2Hf_2O_7$, $Nd_2Hf_2O_7$, $Sm_2Hf_2O_7$ and $Eu_2Hf_2O_7$. One notes the presence of negative phonon frequencies, indicating that the studied pyrochlore compounds $La_2Hf_2O_7$, $Nd_2Hf_2O_7$, $Sm_2Hf_2O_7$ and $Eu_2Hf_2O_7$ are dynamically unstable (see Fig. 3).

3.2. Elastic properties

Elastic properties of a cubic crystal are characterized by three elastic constants, namely, C_{11}, C_{12} and C_{44}. The calculated elastic constants (C_{ij}s) for the studied hafnium oxides are collected in Table 5. From the obtained results, we can make the following conclusions:

(i) The calculated C_{ij}s satisfy the Born's mechanical stability conditions for a cubic system [28]: $C_{11} > 0$, $C_{44} > 0$, $C_{11} > |C_{12}|$, $(C_{11} + 2C_{12}) > 0$. Therefore, it can be concluded that the examined compounds with pyrochlore structure are mechanically stable.
(ii) C_{11}, C_{12} and C_{44} decrease when one moves from $La_2Hf_2O_7$ to $Nd_2Hf_2O_7$ to $Sm_2Hf_2O_7$ to $Eu_2Hf_2O_7$.
(iii) C_{11}, which characterizes the resistance to the uniaxial compression along the [100]/[100]/[100] crystallographic direction [29,30], decreases when moves from $La_2Hf_2O_7$ to $Nd_2Hf_2O_7$ to $Sm_2Hf_2O_7$ to $Eu_2Hf_2O_7$.
(iv) C_{44}, which is related to the resistance to monoclinic shear deformation along the (100) plane of a cubic structure, decreases in the following sequences: $La_2Hf_2O_7 \rightarrow Nd_2Hf_2O_7 \rightarrow Sm_2Hf_2O_7 \rightarrow Eu_2Hf_2O_7$.
(v) The isotropic elastic moduli of the polycrystalline phase of a solid, namely, the bulk (B) and shear (G) moduli, can be calculated from the single crystal elastic constants through the well-known Voigt-Reuss-Hill approximations [31–33]. The Voigt (B_V) and Reuss (B_R) bulk modulus and Voigt (G_V)

Table 4
Calculated Raman and infrared inactive phonon modes (in cm^{-1}) for the $Ln_2Hf_2O_7$ (Ln = La, Nd, Sm and Eu) compounds along with available previous theoretical data.

System	F_{1g} (1)	F_{1g} (2)	A_{2u} (1)	A_{2u} (2)	A_{2u} (3)	E_u (1)	E_u (2)	E_u (3)	$F_{2u}(1)$	$F_{2u}(2)$	$F_{2u}(3)$	$F_{2u}(4)$
$La_2Hf_2O_7$												
This work	585	278	381	279	205	338	156	85	589	291	105	49
Cal. [19]	593	266	363	275	208	326	149	86	573	284	108	52
Cal. [17]	435	301	320	124	70	471	165	99	553	453	187	139
$Nd_2Hf_2O_7$												
This work	609	274	382	265	207	349	146	86	618	304	106	48
Cal. [19]	618	266	369	259	213	340	133	88	605	296	108	52
Cal. [17]	434	294	312	131	67	477	161	100	464	445	190	137
$Sm_2Hf_2O_7$												
This work	635	268	386	252	210	351	127	87	632	309	107	47
Cal. [19]	628	264	372	247	214	346	122	87	628	264	107	50
Cal. [17]	442	294	313	138	65	476	165	99	578	454	187	140
$Eu_2Hf_2O_7$												
This work	641	265	390	248	212	353	119	86	635	315	106	46
Cal. [21]	633	263	373	243	215	350	117	87	628	307	107	50
Cal. [17]	443	297	305	137	66	477	164	99	574	455	192	140

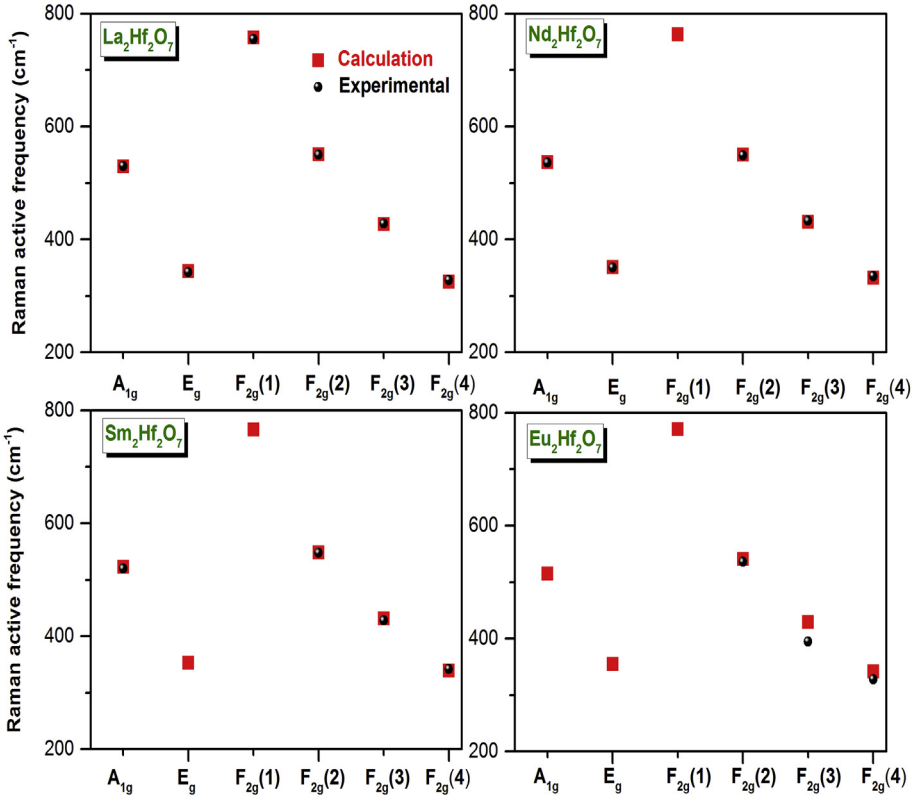

Fig. 2. Theoretical and experimental Raman phonon modes for the $La_2Hf_2O_7$, $Nd_2Hf_2O_7$, $Sm_2Hf_2O_7$ and $Eu_2Hf_2O_7$ compounds.

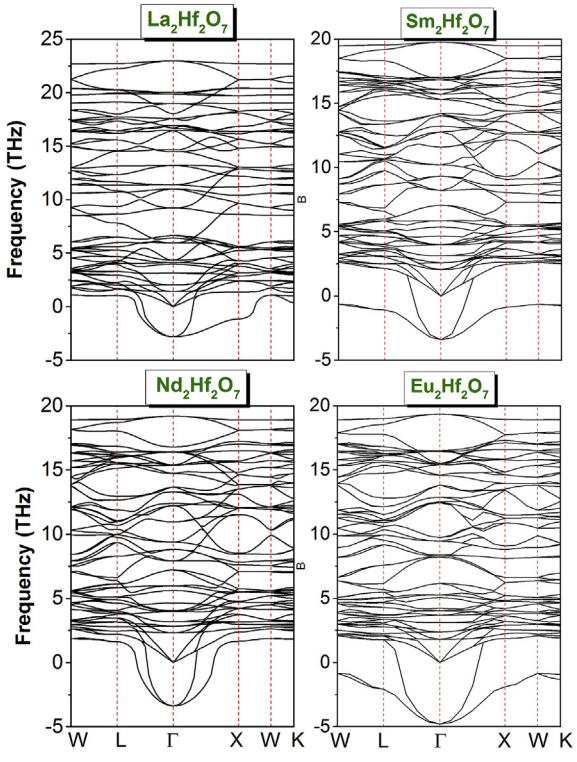

Fig. 3. Phonon dispersion spectra for the $La_2Hf_2O_7$, $Nd_2Hf_2O_7$, $Sm_2Hf_2O_7$ and $Eu_2Hf_2O_7$ compounds.

and Reuss (G_R) shear modulus can be calculated from the C_{ij}s via the following relationships:

$$B = B_V = B_R = (C_{11} + 2C_{12}) / 3$$

$$G_V = (C_{11} - C_{12} + 3C_{44}) / 5$$

$$G_R = \{5(C_{11} - C_{12})\, C_{44}\} / \{4C_{44} + 3(C_{11} - C_{12})\}$$

$$G = (G_V + G_R) / 2$$

The calculated values for the aforementioned elastic moduli for the examined compounds are collected in Table 5. The calculated results are in acceptable agreement with previously calculated results for $La_2Hf_2O_7$. There are no experimental results for the examined compounds to be compared with our results.

(vi) The resistance of a solid against a uniaxial deformation is represented by the Young's modulus E. The Young's modulus can be calculated from B and G through the following relation: $E = 9GB/(3B + G)$. The obtained results are collected in Table 5.

(vii) The interatomic bonding in a material is of covalent nature if the Poisson's ratio σ ($\sigma = (1/2)(3B\text{-}2G)(3B + G)^{-1}$) is equal to 0.1, and it is of ionic character if $\sigma = 0.25$ [34]. Calculated values of the Poisson's ratio reveal that the interatomic bonding in the examined compounds is rather of ionic nature.

(viii) According to an empirical criterion by Pugh, a solid is ductile if B/G ratio is smaller than 1.75; otherwise it is brittle [35,36].

Table 5
Calculated single elastic constants (C_{ij}, in GPa), Bulk modulus (B, in GPa), shear modulus (G, in GPa) Young's modulus (E, in GPa) Poisson's ration (σ, dimensionless), Ziner facor (A^Z, dimensionless) and universal anisotropy factor (A^U, dimensionless) for the $Ln_2Hf_2O_7$ (Ln = La, Nd, Sm and Eu) pyrochlore along with available previous theoretical data.

	C_{11}	C_{12}	C_{44}	B	G	B/G	E	σ	A^Z	A^U
$La_2Hf_2O_7$										
This work	308	115	89	179.33	91.87	1.952	235.41	0.5959	0.9223	0.014
Cal. [7]	286	126	94	180	88		228			
$Nd_2Hf_2O_7$										
This work	301	109	86	173	89.90	1.924	229.88	0.5677	0.8958	0.016
$Sm_2Hf_2O_7$										
This work	297	106	84	169.67	88.43	1.919	226.02	0.5550	0.8796	0.019
$Eu_2Hf_2O_7$										
This work	295	104	83	167.67	87.80	1.902	227.78	0.5445	0.8691	0.023

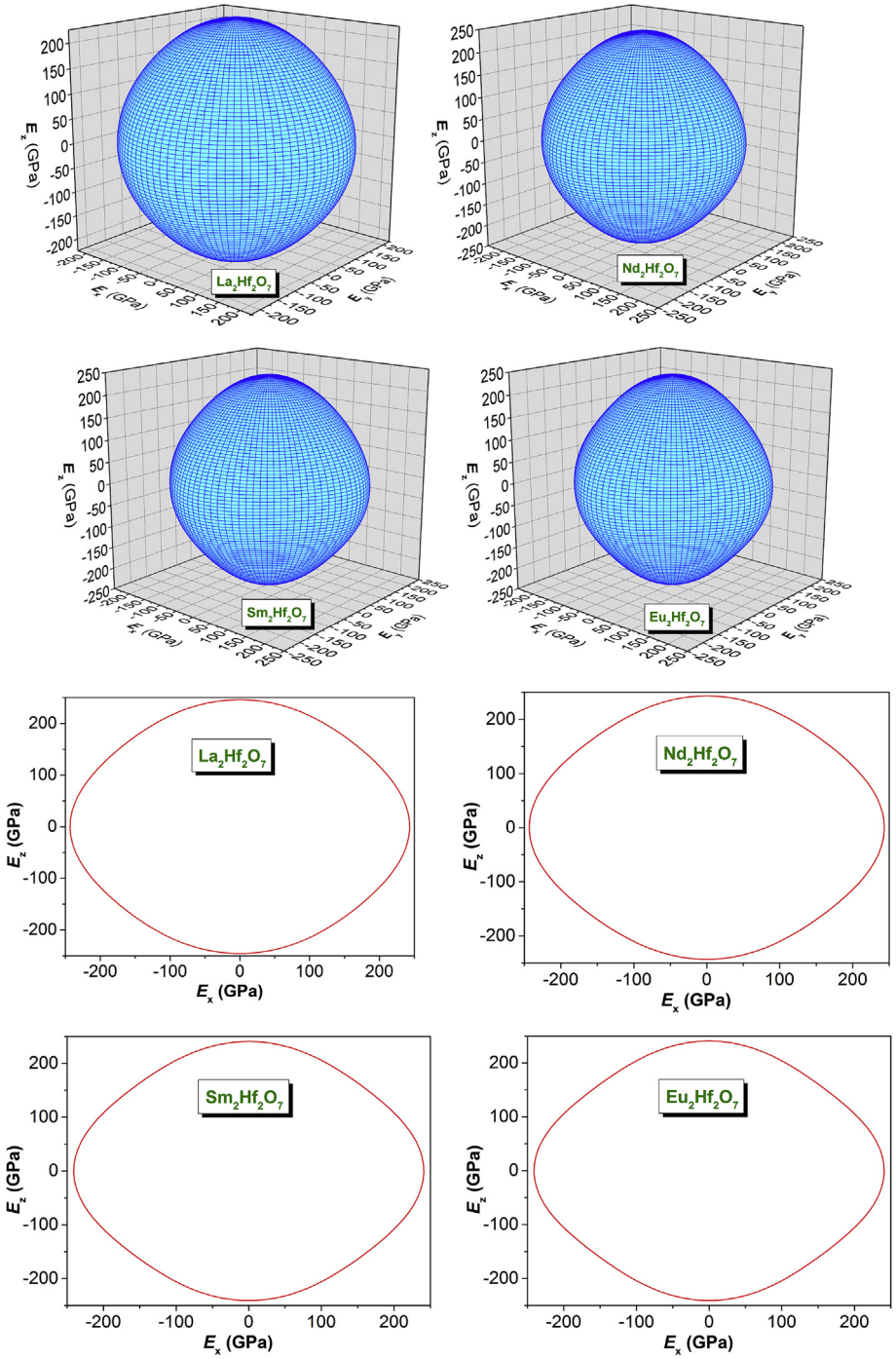

Fig. 4. The calculated three-dimensional stereograms of the Young's modulus and their cross-sections in the *xz*-plane for the $Ln_2Hf_2O_7$ (Ln = La, Nd, Sm and Eu) compounds.

Calculated values of the B/G ratio of the examined compounds, documented in Table 5, reveal that the title compounds are ductile and the ductility decreases when one moves from La to Eu. Moreover, Cauchy pressure ($C_{11}-C_{44}$) is also a criterion that determines the ductile or brittle nature of materials [37–39]. If the value of Cauchy pressure is positive, the material is ductile; otherwise it is brittle. All calculated values of Cauchy pressure are positive, conforming the ductility of the considered compounds.

(ix) From Table 5, it is observed that the interatomic interactions for the examined compounds are not centro-symmetric due to the fact that C_{11} and C_{44} elastic constants are not equal to each other ($C_{11} \neq C_{44}$). Therefore, we can say that the mechanical properties of the examined compounds are directional dependent.

Elastic anisotropy is an important property for the engineering and solid state physicist since it gives insight about the possibility of apparition of micro cracks in materials [20,40]. Some indexes are usually used to evaluate the elastic anisotropy degree. Four different criteria were used to characterize the elastic anisotropy of the title compounds:

(1) The Zener anisotropy A^Z, which is defined as $A^Z = 2C_{44}(C_{11}-C_{12})^{-1}$, gives information about the degree of elastic anisotropy of cubic crystals. If $A^Z = 1$, the material is elastically isotropic, otherwise it has a certain elastic anisotropy. The obtained results indicate that the examined compounds show certain elastic anisotropy which increases when going from La to Eu.

(2) The universal anisotropy factor A^U [41,42], defined as: $A^U = 5\,G_V/G_R + B_V/B_R - 6$, is widely used to evaluate the elastic anisotropy of materials. Calculated values for A^U, listed in Table 5, indicate that the studied compounds exhibit certain elastic anisotropy.

(3) Elastic anisotropy of solids can be evaluated through three dimension (3D) representation of the directional dependence of the elastic moduli, such as the Young's modulus (E). Crystallographic direction dependence of the Young's modulus E is given by the following expression [43]:

$$1 \Big/ E = S_{11} - 2(S_{11} - S_{12} - 0.5S_{44})\left(l_1^2 l_2^2 + l_2^2 l_3^2 + + l_1^2 l_3^2\right)$$

Here, l_1, l_2 and l_3 are the directional cosines with respect to the x-, y- and z-axes, respectively, and S_{ij} are the elastic compliances. For an elastically isotropic material, the 3D-closed surface representing the directional dependence of E has a perfect spherical shape. Thus, the magnitude of deviation of the 3D-closed surface from the sphericity is a measure of the degree of the elastic anisotropy [44]. Computed 3D-closed surfaces for the Young's modulus and their cross-sections in the xz plane for the title compounds are depicted in Fig. 4. One can clearly observe that the shapes of 3D-closed surfaces (their cross section) noticeably deviate from the spherical shape (the circular shape), indicating a pronounced elastic anisotropy in the title compounds.

4. Conclusions

In summary, the developed eight parameter rigid ion model was used to calculate the elastic constants, mechanical properties and zone-centre phonon modes for the hafnium oxides: $La_2Hf_2O_7$, $Nd_2Hf_2O_7$, $Sm_2Hf_2O_7$ and $Eu_2Hf_2O_7$. The main obtained results are:

(i) Calculated single elastic constants (C_{ij}) indicate that the studied compounds are mechanically stable. Calculated elastic moduli, including the C_{ij} and, bulk and shear moduli, decrease in the following sequence: $La_2Sn_2O_7 \rightarrow Nd_2Sn_2O_7 \rightarrow Sm_2Sn_2O_7 \rightarrow Eu_2Sn_2O_7$. Our results for the elastic moduli are very close to those reported in the scientific literature.

(ii) Raman and infrared active and inactive modes of the examined compounds were calculated and the obtained results compare very well to previous results, demonstrating the success of the used model.

References

[1] A.P. Ramirez, Annu. Rev. Mater. Sci. 24 (1994) 453.
[2] B.D. Gaulin, Hyperfine Interact. 85 (1994) 159.
[3] P. Schiffer, A.P. Ramirez, Commun. Cond. Mater. Phys. 10 (1996) 21.
[4] J.E. Greedan, J. Mater. Chem. 11 (2001) 37.
[5] A.P. Ramirez, Handb. Magn. Mater. 13 (2001) 423.
[6] S.T. Bramwell, M.J.P. Gingras, Science 294 (2001) 1495.
[7] R. Vassen, X. Cao, F. Tietz, D. Basu, D. Stover, J. Am. Ceram. Soc. 83 (2000) 2023.
[8] D.P. Cann, C.A. Randall, T.R. Shrout, Solid State Commun. 100 (1996) 529.
[9] K.J.D. Vries, T.V. Dijk, A.J. Burggraaf, Fast Ion Transport in Solids, Amsterda: Elsevier, North Holland, 1979.
[10] R.C. Ewing, W.J. Weber, J. Lian, J. Appl. Phys. 95 (2004) 5949.
[11] S.J. Korf, H.J.A. Koopmans, B.C. Lippens, A.J. Burggrasst, P.J. Gellings, J. Chem. Soc. Faraday. Trans. 83 (1987) 1485.
[12] M. Hanawa, J. Yamaura, Y. Muraoka, F. Sakai, Z. Hiroi, J. Phys. Chem. Solids 63 (2002) 1027.
[13] G.S.V. Coles, S.E. Bond, Williams, J. Mater. Chem. 4 (1994) 23.
[14] S. Fujihara, K. Tokumo, Chem. Mater. 17 (2005) 5587.
[15] A. Zhang, M.L.Z. Yang, G. Zhou, Y. Zhou, Solid State Sci. 10 (2008) 74.
[16] R.C. Ewing, W.J. Weber, J. Lian, J. Appl. Phys. 95 (2004) 5949.
[17] H.C. Gupta, S. Brown, N. Rani, V.B. Gohel, J. Phys. Chem. Solids 63 (2002) 535.
[18] Z. Qi, X. Cheng, B. Liu, G. Zhang, Y. Chen, C. Li, M. Yin, Solid State Commun. 151 (2011) 1288.
[19] S. Kumar, H.C. Gupta, Solid State Sci. 14 (2012) 1405.
[20] B. Liu, J.Y. Wang, F.Z. Li, Y.C. Zhou, Acta Mater. 58 (2010) 4369.
[21] J. Feng, B. Xiao, C.L. Wan, Z.X. Qu, Z.C. Huang, J.C. Chen, R. Zhou, W. Pan, Acta Mater. 59 (2011) 1742.
[22] J. Feng, B. Xiao, R. Zhou, W. Pan, Scr. Mater. 68 (2013) 727.
[23] A.W. Sleight, Inorg. Chem. 7 (1969) 1704.
[24] B.P. Mandal, N. Garg, S.M. Sharma, A.K. Tyagi, J. Solid State Chem. 179 (2006) 1990.
[25] M.A. Subramanian, G. Aravamudan, G.V.S. Rao, Prog. Solid State Chem. 15 (1983) 55.
[26] S. Kumar, H.C. Gupta, Vib. Spectrosc. 62 (2012) 180.
[27] H.C. Gupta, S. Brown, N. Rani, V.B. Gohel, J. Raman Spectrosc. 32 (2001) 41.
[28] J. Wang, S. Yip, S.R. Phillpot, D. Wolf, Phys. Rev. Lett. 71 (1993) 4182.
[29] M. Mattesini, R. Ahuja, B. Johansson, Phys. Rev. B 68 (2003) 184108.
[30] X.P. Gao, Y.H. Jiang, R. Zhou, J. Feng, J. Alloy. Comp. 587 (2014) 819.
[31] W. Voigt, Lehrbuch de Kristallphysik, Terubner, Leipzig, 1928.
[32] A. Reuss, Z. Angew, Math. Mech. 9 (1929) 49.
[33] R. Hill, Proc. Phys. Soc. Lon. Sec. A 65 (1952) 349.
[34] V.V. Bannikov, I.R. Shein, A.L. Ivanovskii, Phys. Status Solidi RRL 3 (2007) 89.
[35] S.F. Pugh, Philos. Mag. 45 (1954) 823.
[36] I.R. Shein, A.L. Ivanovskii, J. Phys. Chem. 20 (2008) 415218.
[37] B. Huang, et al., J. Alloy. Comp. 635 (2015) 213.
[38] J.J. Lewandowski, W.H. Wang, A.L. Greer, Philos. Mag. Lett. 85 (2005) 77.
[39] D.G. Pettifor, Mater. Sci. Technol. 8 (1992) 345.
[40] V.V. Bannikov, I.R. Shein, A.L. Ivanovskii, Phys. Status Solidi 3 (2007) 89.
[41] S.I. Ranganathan, M.O. Starzewski, Phys. Rev. Lett. 101 (2008), 055504.
[42] S.H. Duan, J. Alloy. Comp. 756 (2018) 40.
[43] J.F. Nye, Properties of Crystals, Oxford University Press, 1985.
[44] A. Benmakhlouf, A. Bentabet, A. Bouhemadou, S. Maabed, R. Khenata, S. Bin-Omran, Solid State Sci. 48 (2015) 72.

Update

Computational Condensed Matter

Volume 27, Issue , June 2021, Page

DOI: https://doi.org/10.1016/j.cocom.2021.e00548

Computational Condensed Matter 27 (2021) e00548

Contents lists available at ScienceDirect

Computational Condensed Matter

journal homepage: http://ees.elsevier.com/cocom/default.asp

Erratum regarding missing Declaration of Competing Interest statements in previously published articles

Declaration of Competing Interest statements were not included in published version of the articles that appeared in previous volumes of Computational Condensed Matter.

Please see the appropriate Declaration of Competing Interest statements below.

S.No	Article Title	Journal Title	Year	Volume	Item/Article Number
1	Effect of orientation and mode of loading on deformation behaviour of Cu nanowires	Computational Condensed Matter	2018	17C	330
2	Decoherence of cooled and trapped polariton under magnetic field	Computational Condensed Matter	2018	14C	134
3	The first principle calculations of magnetic and thermoelectric properties of Ba2CeCoO6 with GGA and mBJ approximations	Computational Condensed Matter	2019	19C	380
4	Investigating the electronic structure of MSi (MÂ = Cr, Mn, Fe & Co) and calculating Ueff & J by using cDFT	Computational Condensed Matter	2018	16C	325
5	Theoretical study of structural, elastic and thermodynamic properties of Cu2MgSnX4 (XÂ = S, Se and Te) quaternary compounds	Computational Condensed Matter	2018	18C	339
6	Half-metallic ferromagnetism in Tc and Ag doped MgO: An ab-initio study	Computational Condensed Matter	2019	20C	386
7	Ab-initio investigation of structural, electronic, magnetic, and thermodynamic properties of XPt3 (X = V, Cr, Mn, and Fe) intermetallic compounds	Computational Condensed Matter	2018	16C	328
8	First principle study of the structural, electronic, vibrational, thermodynamic, linear and nonlinear optical properties of zinc-blende ZnSe and ZnTe semiconductors	Computational Condensed Matter	2019	19C	372
9	Ab-initio DFT based investigation of double perovskite oxide Ba2CdOsO6 with cubic structure	Computational Condensed Matter	2018	18C	351
10	Investigation of new d0 half-metallic full-heusler alloys N2BaX (X = Rb, Cs, Ca and Sr) using first-principle calculations	Computational Condensed Matter	2019	19C	371
11	First Brillouin zone-centre phonon frequencies and elastic stiffness of the Ln2Hf2O7 (LnÂ = La, Nd, Sm and Eu) pyrochlore	Computational Condensed Matter	2019	21C	428
12	First-principles study on structural, mechanical, and magneto-electronic properties in new half-metallic perovskite LiBeO3	Computational Condensed Matter	2019	21C	399
13	Effect of pressure and Hubbard potential on the electronic and magnetic properties of thorium monopnictides ThPn (PnÂ = N, P, As, Sb, Bi) in respect of crystal field splitting, charge transfer and spin flipping of magnetic moments	Computational Condensed Matter	2019	21C	403
14	Electronic structure of alumina doped by light elements	Computational Condensed Matter	2018	15C	146
15	First principle studies on structure, magneto-electronic and elastic properties of photovoltaic semiconductor halide (RbGeI3) and ferromagnetic half metal oxide (RbDyO3)	Computational Condensed Matter	2019	19C	381

The authors were contacted after publication to request a Declaration of Interest statement.

The authors declare that they have no known competing financial interests or personal relationships that could have appeared to influence the work reported in this paper.

DOIs of original article: https://doi.org/10.1016/j.cocom.2018.e00325, https://doi.org/10.1016/j.cocom.2018.e00328, https://doi.org/10.1016/j.cocom.2019.e00371, https://doi.org/10.1016/j.cocom.2019.e00428, https://doi.org/10.1016/j.cocom.2019.e00399, https://doi.org/10.1016/j.cocom.2018.03.007, https://doi.org/10.1016/j.cocom.2018.e00351, https://doi.org/10.1016/j.cocom.2019.e00372, https://doi.org/10.1016/j.cocom.2019.e00386, https://doi.org/10.1016/j.cocom.2019.e00381, https://doi.org/10.1016/j.cocom.2018.e00330, https://doi.org/10.1016/j.cocom.2019.e00380, https://doi.org/10.1016/j.cocom.2018.e00339, https://doi.org/10.1016/j.cocom.2019.e00403, https://doi.org/10.1016/j.cocom.2018.01.012.

https://doi.org/10.1016/j.cocom.2021.e00548